




**Magnon polarons induced by a magnetic field gradient**N. Vidal-Silva <sup>1,2,\*</sup>,† E. Aguilera <sup>3,\*</sup> A. Roldán-Molina,<sup>4</sup> R. A. Duine,<sup>5,6,7</sup> and A. S. Nunez<sup>2,3</sup><sup>1</sup>*Departamento de Ciencias Físicas, Universidad de La Frontera, Casilla 54-D, 4811186 Temuco, Chile*<sup>2</sup>*CEDENA, Universidad de Santiago de Chile, Avenida Ecuador 3493, Santiago, Chile*<sup>3</sup>*Departamento de Física, FCFM, Universidad de Chile, Santiago, Chile*<sup>4</sup>*Universidad de Aysén, Calle Obispo Vielmo 62, Coyhaique, Chile*<sup>5</sup>*Institute for Theoretical Physics, Utrecht University, 3584CC Utrecht, The Netherlands*<sup>6</sup>*Department of Physics, Center for Quantum Spintronics, Norwegian University of Science and Technology, NO-7491 Trondheim, Norway*<sup>7</sup>*Department of Applied Physics, Eindhoven University of Technology, P.O. Box 513, 5600 MB Eindhoven, The Netherlands* (Received 16 June 2020; revised 24 August 2020; accepted 25 August 2020; published 8 September 2020)

In this paper, we report the theoretical possibility of generating magnon-polaron excitations through a space-varying magnetic field. The spatial dependence of the magnetic field in the Zeeman interaction gives rise to a magnon-phonon coupling when a magnetic field gradient is applied, and such a coupling depends directly on the strength of the gradient. It is also predicted that the direction of the magnetic field gradient allows control over which phonon polarization couples to the magnons in the material. Here, we develop the calculations of the magnon-phonon coupling for an arbitrary (anti)ferromagnet, which are later used to numerically study its consequences. These results are compared to the ones obtained with the phenomenological magnetoelastic coupling in yttrium iron garnet (YIG) where we show that the magnon-polaron band gap seen in YIG can be also obtained with a magnetic field gradient of  $\sim 0.1$  T/m which can be achieved with the current experimental techniques. Our results propose a different way of controlling the magnetoelastic coupling in an arbitrary material and open a route to exploit the magnon-phonon interaction in magnonic and spintronic devices.

DOI: [10.1103/PhysRevB.102.104411](https://doi.org/10.1103/PhysRevB.102.104411)**I. INTRODUCTION**

In the past years, the magnetoelastic coupling has gained much attention due to the potential applications it offers in the field of spintronics [1–3], magnonics [4,5], spin caloritronics [6], and, more recently, spin mechatronics [7]. The simultaneous excitation of spin and elastic waves mediated by the magnetoelastic coupling gives rise to the so-called magnetoelastic waves [8,9], which has been a focus of study over the past decades [10–12]. However, due to recent progress in the synthesis and characterization techniques of materials, the effects related to the magnetoelastic coupling have been experimentally better addressed only recently [13–16].

From a quantum-mechanical point of view, both spin and elastic waves have a quantized form of their elementary excitations, namely, magnons and phonons, respectively. Due to their bosonic nature, both quasiparticles obey the Bose-Einstein statistics. In the long-wave-length limit and around the  $\Gamma$  point, magnons in collinear ferromagnets are usually characterized by their quadratic dispersion relation, which possesses a band gap proportional to the external magnetic field and the magnetic anisotropy [17]. Differently, magnons in antiferromagnets present a linear dispersion relation around the same point [18]. On the other hand, phonons have a well-known linear dispersion at low energy and, according to the symmetry of the material, have three distinct vibrational

modes [19]. In the absence of magnetoelastic coupling, the dispersion relations of the magnon and phonon might cross at some wave-vector  $\mathbf{k}^*$ . However, in the presence of magnetoelastic coupling, the interaction between magnons and phonons avoids the *crossing point* at  $\mathbf{k}^*$ , and, instead, forms what is called an *anticrossing point* [20–23]. At this point, the interaction between magnons and phonons is maximum, and the related eigenstates are a hybridization between magnons and phonons, called magnon polarons or magnetoelastic waves [23–25].

Magnon polarons have recently been studied in the context of transport, topological, and magnetic properties of, mainly, (anti)ferromagnetic insulators. For example, anomalies in the spin Seebeck [26] and spin Peltier [27] effects have been attributed to the presence of magnon polarons. Local [23,26] and nonlocal [28,29] magnon-polaron spin transport has been also studied and/or measured in yttrium iron garnet (YIG) films. More recently, the topological nature of magnon-polarons has been predicted [14,30–32] as well as the control of its topology [30,33]. Antiferromagnets also present magnon-polarons as reported in Refs. [34,35]. Particularly, noncollinearity in antiferromagnets has been pointed out as a source of magnon-polaron excitations [35]. Spin pumping has been also enhanced due to the presence of magnon-polarons [36]. Thus, in most of the effects attributed to magnon-polarons, the magnitude of its contribution depends essentially on the magnetoelastic parameter, which quantifies the strength of the interaction. For instance, in Ref. [37], the nonreciprocity of the sound velocity in the phonon magneto-chiral effect is mediated by the cubic of a magnetoelastic

\*N.V.-S. and E.A. contributed equally to this paper.

†Corresponding author: nicolas.vidal@ufrontera.cl

constant. In the same way, the magnon lifetime due to the phonon scattering is also proportional to the magnetoelastic constant [22,38]. The enhancement of magnetization damping by phonon pumping has been reported to be proportional to the magnetoelastic constant too [39]. In general, any physical quantity related to the action of magnon-polarons depends on a magnetoelastic parameter. Importantly, the strength and source of this interaction are not unique: Although there is an intrinsic anisotropy-mediated magnetoelastic coupling, hereafter, phenomenological magnetoelastic coupling, which stems from the spin-orbit coupling and dipole-dipole interaction [11,12], there are also other sources of magnetoelastic coupling as the dependence of the exchange interaction on the lattice deformations [20,22,38,40] or the modulation of the Dzyaloshinskii-Moriya (DM) interaction by shear strains [14,15,37].

In this paper, we study how a magnetoelastic coupling can be induced by applying a magnetic field gradient on a arbitrary magnetic lattice. We will show analytically and numerically that the coupling depends directly on the magnitude and direction of the magnetic field gradient. This will be shown to imply that the experimental control of the magnetic field's shape allows the tuning of the coupling strength and the possibility of selecting which phonon polarization couples to the magnons of the material. The presented coupling could be applied, in principle, to any (anti)ferromagnetic lattice with a crossing point between the dispersion relations of magnons and phonons. The idea of controlling the magnon-phonon coupling with inhomogeneous magnetic fields [20,41–43], time-dependent magnetic fields [21,44], or other methods [45,46] has been already reported in the literature where the main idea is to control the magnon dispersion to make it match with the phonon one, obtaining, thus, a controllable magnon-phonon coupling with a constant strength, which is mediated by a magnetoelastic constant. However, our proposal goes beyond the mentioned approaches. Specifically, we claim to control the magnon-phonon interaction not only by choosing when magnon and phonon bands hybridize through the gradient direction, but also to control the strength of the interaction that results to be directly proportional to the module of the magnetic field gradient as will be shown below.

The paper is organized as follows: In Sec. II, we start our paper by describing the proposal with a toy model in a unidimensional system. Despite this is a pretty simple model, it will allow us to establish the role that a magnetic field gradient plays in the stability of a given system in the presence of an inhomogeneous magnetic field with the same periodicity of the lattice. Once we identify the conditions that our system must have in order to be physically realizable, in Secs. II A and II B, we introduce the basic concepts on the quantization of the magnetic and elastic systems in a superlattice, respectively, and explore the analytical nature of the magnon-phonon coupling due to a magnetic field gradient in Sec. II C. Also, in Sec. II D, we detail the numerical algorithm we used to diagonalize the Hamiltonian of our system. Next, in Sec. III, we apply our results to a magnonic crystal where we study the dispersion relation of magnon-polarons and highlight the main properties of the energy bands obtained with the proposed coupling mechanism. We also make a comparison between

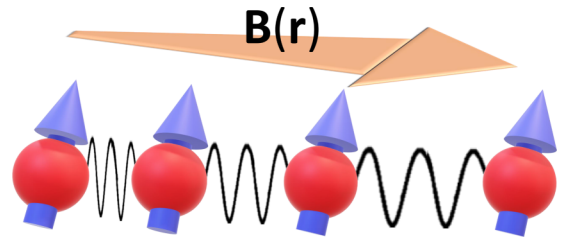


FIG. 1. Schematic of the unidimensional lattice with a space-varying magnetic field. The nonuniform arrow represents a magnetic field gradient, which according to our proposal, exerts an external force on each magnetic dipole which deviates them from its equilibrium position so ultimately excites simultaneously magnon and phonon modes, generating, thus, magnon-polaron excitations.

the phenomenological magnetoelastic coupling and the one we propose. Finally, in Sec. IV, we discuss and give some conclusions for future works.

## II. MODEL

In this section, we will describe the nature of magnons and phonons in an arbitrary lattice as well as their coupling due to the enforcement of a magnetic field gradient in the presence of a space-varying magnetic field. We chose to explore our proposal utilizing a lattice model in a quantum-mechanical frame. However, it is essential to keep in mind that a continuous model should work as well, and in such a case, the energy of a continuous elastic theory with a continuous spin field must be employed. For simplicity, we will assume a low-temperature regime such that the magnetization's fluctuations are weak enough to keep the magnetic order with no thermal disturbance. The idea of this section is to capture the physics behind the magnetic field gradient-mediated magnon-phonon coupling considering an inhomogeneous magnetic field with the same periodicity of the lattice. This will allow us to understand the physical limitations of the proposal, and it will pave our way to the next section where we will overcome some of these limitations by changing the spatial periodicity of the magnetic field. We will also consider a ferromagnetic insulator to neglect the electronic charge.

As mentioned before, we will begin by analyzing a unidimensional magnetoelastic lattice with nearest-neighbor distance  $a_0$  in a space-varying magnetic field  $\mathbf{B}(\mathbf{r})$  with the same periodicity of the lattice. For this first example, we will consider that the system is dominated by a nearest-neighbor elastic coupling, nearest-neighbor Heisenberg exchange, and Zeeman interaction as depicted in Fig. 1. In this way, we consider a spin chain along the  $x$  axis and parametrize the Hamiltonian of it in terms of the displacement  $u_i = x_i - X_i$ , being  $x_i$  and  $X_i$ , the position and equilibrium position of site  $i$ , respectively; the phonon momentum  $p_i$ , and the spin vectors  $\mathbf{S}_i$ , meaning that the Hamiltonian reads

$$\mathcal{H} = \sum_{i=1}^N \left[ \frac{p_i^2}{2M} + \frac{M\omega_0^2}{2} (u_{i+1} - u_i)^2 - \mathbf{J} \mathbf{S}_i \cdot \mathbf{S}_{i+1} - \mu_B g \mathbf{B}(x_i) \cdot \mathbf{S}_i \right], \quad (1)$$

where  $J$  is the Heisenberg exchange constant,  $M$  is the average mass of each site,  $\omega_0$  is the natural frequency of the elastic coupling between two neighboring sites,  $\mu_B$  is the Bohr magneton, and  $g$  is the Landé factor.

We can expand the magnetic field around its equilibrium  $X_i$  up to first order in the displacement  $u_i$  in the displaced position  $x_i = X_i + u_i$ ,

$$B^\alpha(x_i) = B^\alpha(X_i) + \left. \frac{\partial B^\alpha}{\partial x} \right|_{x=X_i} u_i + O(u_i^2). \quad (2)$$

Note that a magnetoelastic coupling has been induced as evidenced in the linear term of the expansion in displacement  $u_i$ . Importantly, the proposed interaction does not have a dependence on the derivative or differences of the displacement field as reported in previous works [11,30,37,38]. This is consistent with the fact that, in the present paper, and due to the application of a magnetic field gradient, every spin in the lattice is subject to a distinct distortion in such a way that the displacement field is different for every site, so each spin displaces differently. In other words, the presented mechanism breaks the translation invariance. This makes the linear term in the displacement field the dominant one. This procedure will be used from now on, and it will be the base to show how a magnetic field gradient drives an induced magnetoelastic coupling. Eq. (2) can be directly replaced on Hamiltonian (1) to obtain

$$\mathcal{H} = \sum_{i=1}^N \left[ \frac{p_i^2}{2M} + \frac{M\omega_0^2}{2} (u_{i+1} - u_i)^2 - JS_i \cdot S_{i+1} - \mu_B g \mathbf{B}(X_i) \cdot \mathbf{S}_i - \mu_B g u_i \mathbf{S}_i \cdot \left. \frac{\partial \mathbf{B}}{\partial x} \right|_{x_i} \right], \quad (3)$$

where the induced magnetoelastic interaction becomes evident in the last term of the above expression when coupling the elastic degrees of freedom  $\{u_i\}$  with the magnetic ones  $\{S_i\}$ . Note that a similar spin-phonon interaction could be obtained following the guidelines of Ref. [47] by manipulating the last term of Eq. (3) to express the coupling in terms of the strain tensor. However, such a formalism does not consider variations on the magnetic field as in the present case and focuses on a lattice with no basis, which differs from this essential feature of our model as we will argue below. This fact imposes that the dominant term does not involve derivatives of the displacement field [see Eqs. (7) and (29)].

Before proceeding onto studying the coupling of magnons and phonons, it is essential to analyze the classical equilibrium of the system. This procedure is crucial because a magnetic field gradient exerts a force on every magnetic dipole, which could change the behavior of its equilibria. To study the equilibria of Hamiltonian (1), the spin variable will be written in terms of its spherical angles  $\phi_i$  and  $\theta_i$ , and it will be assumed that the magnetic field is given by  $\mathbf{B}(x) = [0, B^y(x), B^z]$ . The main idea is, then, to write down the Hamiltonian (1) as a function of the variables  $\{\theta_i, \phi_i, u_i\}$  and after Fourier transform the resulting Hamiltonian, minimize it respect to the variables  $\{u_k, u_{-k}, \theta_k, \theta_{-k}\}$ . Major details about the equilibrium analysis at this stage can be found in Appendix A. Thus, it can be proven that every eigenvalue of Eq. (1) is positive if and

only if,

$$\left[ Sg\mu_B \frac{\partial B^y}{\partial x} \right]^2 < 4SM\omega_0^2 [-2JS + 2JS \cos(a_0k) + \mu_B g B^z] \sin^2 \left( \frac{ka_0}{2} \right). \quad (4)$$

It is essential to recall that a stable equilibrium is obtained if every eigenvalue of the Hessian is positive, which is reflected in inequality Eq. (4). In this particular case, it must be noted that there exists, at least, a value of  $k$  such that inequality (4) is not satisfied, meaning that the system is not in the real ground state so that the equilibrium analysis was performed in an excited state and, then, it is unstable. This can be understood in terms of the appearance of a force related to the application of the magnetic field gradient, which acts on each spin pushing them out of the equilibrium and ultimately accelerates the system. An accelerated system is no longer at stable equilibrium, and, then, the real equilibrium state must be achieved. Equation (4) says that, for some range of  $k$  values, this new equilibrium state will never be reached, which means that magnons and phonons at that regime are unstable and no magnetoelastic coupling it would be observed as shown in Fig. 5 of Appendix A. Thus, by choosing a magnetic field with the same periodicity of the lattice, whatever be the magnetic field gradient applied, the spins equilibrium position, or the magnetic ground state, the system will always show nonequilibrium aspects and then magnon-polaron excitations are not allowed. To overcome this issue and obtain stable magnon-polarons in the entire first Brillouin zone, we need that an opposite force acts on the system and cancels the acceleration. For such a purpose, we are going to study the problem of these hybridized quasiparticles in an arbitrary lattice composed of  $N$  unit cells with a basis of  $m$  sites, which will allow us to adapt the magnetic field to get a stable configuration. In other words, by modifying the magnetic field periodicity, we can control how many spins belong to the new unit cell of the lattice so that the purpose of canceling the acceleration on the system relies now on canceling the net force on each unit cell. Thus, the needed force to canceling the acceleration of the system emerges from the shape and periodicity of the magnetic field. To be more specific, in the particular case, we will examine the magnetic field will be adjusted such that the gradient applied to it translates into a force pointing in a given direction acting on the half of spins in the unit cell, whereas the other half is under the action of an opposite force, achieving, thus, the equilibrium on the system. It is important to recall that the premise of our model is, then, to modulate the magnetic field such that the forces that emerge from the gradient are always accompanied by an opposite one (which emerges from the gradient too) to ensure the acceleration of the system is identically nulled.

We will separate the study of the total Hamiltonian in an arbitrary lattice into three partial Hamiltonians,

$$\mathcal{H} = \mathcal{H}_m + \mathcal{H}_{ph} + \mathcal{H}_{mp}. \quad (5)$$

In Hamiltonian  $\mathcal{H}_m$ , we will include the magnon terms, which will come from the Heisenberg exchange and the zeroth-order expansion of the magnetic field in the Zeeman term. In  $\mathcal{H}_{ph}$ , we will consider the purely phononic terms, which come from

the kinetic energy and a elastic potential.  $\mathcal{H}_{mp}$  includes the term that couple magnons and phonons, which will come from the first-order expansion in the displacement of the Zeeman energy.

### A. Magnons

Magnons are the bosonic elementary excitations of magnetic order, and they are usually interpreted as the quanta of spin waves [48]. This system will be under the influence of an anisotropic exchange interaction and the Zeeman interaction with the external magnetic field. With this, we have that the Hamiltonian reads

$$\mathcal{H} = -\frac{1}{2} \sum_{i'i'jj'} S_{ij}^\alpha J_{i-i'}^{jj'\alpha\beta} S_{i'j'}^\beta - \mu_{BG} \sum_{ij} \mathbf{B}(\mathbf{r}_{ij}) \cdot \mathbf{S}_{ij}, \quad (6)$$

where summation over repeated greek indices is implied throughout this article and in this case  $\alpha, \beta \in \{\hat{x}, \hat{y}, \hat{z}\}$ . The indices  $i, i' \in \{1, 2, \dots, N\}$  and  $j, j' \in \{1, 2, \dots, m\}$  represent the unit cells and basis sites, respectively, and  $i - i' \equiv \mathbf{R}_i - \mathbf{R}_{i'}$  is the distance between nearest-neighbor unit cells. Note that the quantities with subindices  $ij$  should be understood as the  $j$ th element (basis site) of the  $i$ th unit cell of the system. In the Hamiltonian, we have also included the tensor  $J_{i-i'}^{jj'}$ , which corresponds to a generalized interaction between sites  $\mathbf{S}_{ij}$  and  $\mathbf{S}_{i'j'}$  with no particular choice of a given symmetry such that it might contain as the nearest-neighbor exchange interaction as well as a DM interaction.

In order to isolate the terms purely related with the magnetic degrees of freedom from the Zeeman term, we will proceed as in Eq. (2) and expand the magnetic field around the equilibrium positions  $\mathbf{R}_{ij}$  up to first order in their displacement  $\mathbf{u}_{ij}$  as

$$\mathbf{B}^\alpha(\mathbf{r}_{ij}) = \mathbf{B}^\alpha(\mathbf{R}_{ij}) + \left. \frac{\partial \mathbf{B}^\alpha}{\partial r^\beta} \right|_{\mathbf{r}_{ij}=\mathbf{R}_{ij}} u_{ij}^\beta + O(u_{ij}^2), \quad (7)$$

where we are going to keep only the first term of the expansion and in Sec. II C, we are going to consider the second one to obtain the magnon-phonon coupling. We will also adopt the notation,

$$\mathbf{B}_j^\alpha \equiv \mathbf{B}^\alpha(\mathbf{R}_{ij}) \quad \text{and} \quad B_j^{\alpha\beta} \equiv \left. \frac{\partial B^\alpha}{\partial r^\beta} \right|_{\mathbf{r}_{ij}=\mathbf{R}_{ij}}. \quad (8)$$

To obtain a quantized magnonic Hamiltonian, we must start by using the Holstein-Primakoff transformation [48], which allows us to write the spin operators  $\mathbf{S}_{ij}$  in terms of bosonic operators  $a_{ij}$  and  $a_{ij}^\dagger$ , which annihilates and creates magnons, respectively. This transformation reads

$$S_{ij}^x \approx \sqrt{\frac{S}{2}} (a_{ij}^\dagger + a_{ij}), \quad (9a)$$

$$S_{ij}^y \approx i\sqrt{\frac{S}{2}} (a_{ij}^\dagger - a_{ij}), \quad (9b)$$

$$S_{ij}^z \approx S - a_{ij}^\dagger a_{ij}, \quad (9c)$$

where we have linearized the spin operators by using the boson operators  $a_{ij}$  ( $a_{ij}^\dagger$ ) described above by considering the  $z$  axis as the quantization axis, according to the linear spin-wave theory. The reason for keeping the linear order for the

$x$  and  $y$  component of spin operators is that, together with the phonon operators, they will give rise to a Hamiltonian in its quadratic form, which is enough to obtain the energy spectrum of the system. Furthermore, we are interested in obtaining the description of magnons in  $\mathbf{k}$  space, which is obtained by employing the Fourier series, given by

$$a_{ij} = \frac{1}{\sqrt{N}} \sum_{\mathbf{k}} a_{\mathbf{k}j} e^{i\mathbf{k} \cdot \mathbf{r}_{ij}}. \quad (10)$$

Now, we can simultaneously replace Eqs. (9) and (10) into Hamiltonian (6) to obtain the Hamiltonian for magnons in  $\mathbf{k}$  space, which reads

$$\begin{aligned} \mathcal{H}_m = & -\frac{S}{4} \sum_{jj'k} [\Gamma_k^{jj'-} a_{\mathbf{k}j}^\dagger a_{-\mathbf{k}j'}^\dagger + \bar{\Gamma}_k^{jj'-} a_{-\mathbf{k}j} a_{\mathbf{k}j'} + \Gamma_k^{jj'+} a_{\mathbf{k}j}^\dagger a_{\mathbf{k}j'}^\dagger \\ & + \bar{\Gamma}_k^{jj'+} a_{-\mathbf{k}j} a_{-\mathbf{k}j'}^\dagger - 2J_0^{jj'zz} (a_{\mathbf{k}j}^\dagger a_{\mathbf{k}j} + a_{\mathbf{k}j'}^\dagger a_{\mathbf{k}j'})] \\ & + \mu_{BG} \sum_{jk} B_j^z a_{\mathbf{k}j}^\dagger a_{\mathbf{k}j}, \end{aligned} \quad (11)$$

where  $\Gamma_k^{jj'\pm}$  and  $\bar{\Gamma}_k^{jj'\pm}$  are defined as

$$\Gamma_k^{jj'\pm} = J_k^{jj'xx} \mp iJ_k^{jj'xy} + iJ_k^{jj'yx} \pm J_k^{jj'yy}, \quad (12a)$$

$$\bar{\Gamma}_k^{jj'\pm} = J_k^{jj'xx} \pm iJ_k^{jj'xy} - iJ_k^{jj'yx} \pm J_k^{jj'yy}, \quad (12b)$$

and

$$J_k^{jj'\alpha\beta} = \sum_{i-i'} J_{i-i'}^{jj'\alpha\beta} e^{i\mathbf{k} \cdot (\mathbf{r}_{ij} - \mathbf{r}_{i'j'})}. \quad (13)$$

Note that Eq. (13) does not represent the Fourier transformation of  $J_{i-i'}^{jj'\alpha\beta}$ , but it is a definition where the summation on  $\mathbf{k}$  by the factor  $\exp(i\mathbf{k} \cdot \mathbf{r}_{ij})$  is inherited from the Fourier transform of Boson operators.

The result obtained in Eq. (11) can be used for any lattice with magnetic order. Even though in Eq. (9) we have assumed that the magnetic order in equilibrium is equal to  $\hat{z}$  for every site in the lattice, we can incorporate any periodic magnetic texture described by the equilibriums  $\mathbf{S}_0(\theta_j, \phi_j)$  (for instance, a skyrmion or vortex lattice) by introducing a local change of coordinates at every site by means of rotation matrices,

$$R_j \equiv \begin{pmatrix} \cos \phi_j & -\sin \phi_j & 0 \\ \sin \phi_j & \cos \phi_j & 0 \\ 0 & 0 & 1 \end{pmatrix} \begin{pmatrix} \cos \theta_j & 0 & \sin \theta_j \\ 0 & 1 & 0 \\ -\sin \theta_j & 0 & \cos \theta_j \end{pmatrix}, \quad (14)$$

which can be used to redefine the anisotropic exchange tensor as

$$\mathcal{J}_{i-i'}^{jj'} = R_j^T J_{i-i'}^{jj'} R_{j'}, \quad (15)$$

where we only have to use  $\mathcal{J}_{i-i'}^{jj'}$  instead of  $J_{i-i'}^{jj'}$  in Eq. (13). An important aspect at this point is that when considering the DM interaction and depending on the anisotropy and the external magnetic field, the magnetic ground state could no longer be collinear, so not only commensurate magnetic structures might appear (for instance, a skyrmion lattice), but also other noncommensurate ones. In such cases, the local rotation presented in Eq. (14) is not enough to diagonalize the Hamiltonian, and a preceding coordinate transformation



involving a rotating frame must be employed by introducing an ordering wave vector [49].

### B. Phonons

Analog to spin waves, elastic waves can also be quantized. The elementary excitations of elastic waves are the so-called phonons. To describe phonons in our system, we consider that each ion with mass  $M$  at position  $\mathbf{r}_{ij}$  deviates from its equilibrium position  $\mathbf{R}_{ij}$  by a small displacement  $\mathbf{u}_{ij} = \mathbf{r}_{ij} - \mathbf{R}_{ij}$  such that the phonon Hamiltonian can be written as [50,51]

$$\mathcal{H}_{ph} = \sum_{ij} \frac{\mathbf{p}_{ij}^2}{2M} + \sum_{ii'jj'} \frac{1}{2} u_{ij}^\alpha \Phi_{i-i'}^{jj'\alpha\beta} u_{i'j'}^\beta, \quad (16)$$

where  $\mathbf{p}_i$  is the conjugate momentum vector and the index convention is the same as used for Eq. (6). Additionally, we have that the mechanical interaction between two sites is described by the elastic tensor  $\Phi_{i-i'}^{jj'\alpha\beta}$ , which can be used to define

$$\Phi_{\mathbf{k}}^{jj'\alpha\beta} = \sum_{\mathbf{k}} \Phi_{i-i'}^{jj'\alpha\beta} e^{i\mathbf{k} \cdot (\mathbf{r}_{ij} - \mathbf{r}_{i'j'})}. \quad (17)$$

The same as in Eq. (13), Eq. (17) does not represent the Fourier transformation of  $\Phi_{i-i'}^{jj'\alpha\beta}$ , but it is a definition where the summation on  $\mathbf{k}$  by the factor  $\exp(i\mathbf{k} \cdot \mathbf{r}_{ij})$  is inherited from the Fourier transform of boson operators. It is also important to note that because  $\Phi_{i-i'}^{jj'\alpha\beta}$  is originally obtained from the second-order expansion of the potential energy between sites  $\mathbf{r}_{ij}$  and  $\mathbf{r}_{i'j'}$  [51], we must have that  $\Phi_{\mathbf{k}}^{jj'\alpha\beta}$  is real and symmetric, which ultimately implies that it is diagonalizable as

$$\Phi_{\mathbf{k}}^{\mu\nu} \epsilon_{k\lambda}^\nu = \phi_{k\lambda} \epsilon_{k\lambda}^\mu, \quad (18)$$

where we have used the indices  $\mu$  and  $\nu$  as a shorthand to represent the basis  $j, j'$  and coordinate  $\alpha, \beta$  as a single index. With the diagonalization of the problem, we obtain  $\lambda \in \{1, 2, \dots, 3m\}$  eigenvalues and eigenvectors. Here, the vectors  $\epsilon_{k\lambda}$  encode the phonon polarizations which can, in turn, be used to write the operators in  $\mathbf{k}$  space using the discrete Fourier transform,

$$u_i^\mu = \frac{1}{\sqrt{N}} \sum_{k\lambda} u_{k\lambda} \epsilon_{k\lambda}^\mu e^{i\mathbf{k} \cdot \mathbf{r}_{ij}}, \quad (19a)$$

$$p_i^\mu = \frac{1}{\sqrt{N}} \sum_{k\lambda} p_{k\lambda} \epsilon_{k\lambda}^\mu e^{i\mathbf{k} \cdot \mathbf{r}_{ij}}. \quad (19b)$$

Replacing Eqs. (19a) and (19b) into Eq. (16) to obtain the Hamiltonian in  $\mathbf{k}$  space yields

$$H_{ph} = \sum_{k\lambda} \left[ \frac{p_{k\lambda} p_{-k\lambda}}{2M} + \frac{M}{2} \omega_\lambda(\mathbf{k}) u_{k\lambda} u_{-k\lambda} \right]. \quad (20)$$

To transform the displacement and momentum operators of Hamiltonian (20) to phonon creation and annihilation operators, we will use the usual transformation,

$$u_{k\lambda} = \sqrt{\frac{\hbar}{2M\omega_\lambda(\mathbf{k})}} (c_{-k\lambda}^\dagger + c_{k\lambda}), \quad (21a)$$

$$p_{k\lambda} = i\sqrt{\frac{\hbar M\omega_\lambda(\mathbf{k})}{2}} (c_{-k\lambda}^\dagger - c_{k\lambda}), \quad (21b)$$

where the operator  $c_{k\lambda}^\dagger$  ( $c_{k\lambda}$ ) creates (annihilates) a phonon with momentum  $\mathbf{k}$  and polarization  $\lambda$  and obeys the usual commutation relations,

$$[c_{k\lambda}, c_{k'\lambda'}^\dagger] = \delta_{\mathbf{k}\mathbf{k}'} \delta_{\lambda\lambda'}, \quad (22a)$$

$$[c_{k\lambda}, c_{k'\lambda'}] = [c_{k\lambda}^\dagger, c_{k'\lambda'}^\dagger] = 0. \quad (22b)$$

Replacing the transformations (21) into Hamiltonian (20), we obtain an already diagonalized form of the phonon Hamiltonian,

$$H_{ph} = \sum_{k\lambda} \hbar\omega_\lambda(\mathbf{k}) \left( c_{k\lambda}^\dagger c_{k\lambda} + \frac{1}{2} \right), \quad (23)$$

where the phonon's dispersion relation is

$$\omega_\lambda(\mathbf{k}) = \sqrt{\frac{\phi_{k\lambda}}{M}}, \quad (24)$$

being  $\phi_{k\lambda}$ , the eigenvalues of the tensor  $\Phi_{\mathbf{k}}^{jj'\alpha\beta}$ . For simplicity, in the numerical calculations of the next section, we will consider an isotropic material. Specifically, we will use sound velocities  $v_\lambda$  reported for YIG samples, which are incorporated to the elastic tensor by setting its Fourier transform equal to

$$\Phi_{\mathbf{k}}^{jj'\alpha\beta} = V^{\alpha\beta} [2 - (1 + e^{-i2k a_0}) \delta_{j,0} \delta_{j',1} - (1 + e^{i2k a_0}) \delta_{j,1} \delta_{j',0}], \quad (25)$$

where

$$V^{\alpha\beta} = \frac{M}{a_0^2} \begin{pmatrix} v_\parallel^2 & 0 & 0 \\ 0 & v_\perp^2 & 0 \\ 0 & 0 & v_\perp^2 \end{pmatrix}. \quad (26)$$

It is crucial to note this particular elastic tensor allows us to recover the well-known phonon's dispersion relation in the long wave-length limit, which is given by

$$\hbar\omega_\lambda(\mathbf{k}) = v_\lambda |\mathbf{k}|, \quad (27)$$

where  $v_\parallel$  corresponds to the sound velocity of the longitudinal mode, whereas  $v_\perp$  corresponds to the transversal mode.

### C. Magnon polarons

The hybridization between magnons and phonons mediated by the magnetoelastic coupling forms the so-called magnon-polarons. They are the quanta of the magnetoelastic waves which are a solution of the coupled set of differential equations involving the magnetic and elastic degrees of freedom [20]. The way we choose to obtain the magnon-polaron excitations is to quantize the total Hamiltonian composed by the magnetic, elastic, and magnetoelastic parts,

$$\mathcal{H} = \mathcal{H}_m + \mathcal{H}_{ph} + \mathcal{H}_{mp}, \quad (28)$$

where  $\mathcal{H}_m$  is given by Eq. (11) and  $\mathcal{H}_{ph}$  by Eq. (23). To obtain the expression of the magnon-phonon Hamiltonian  $\mathcal{H}_{mp}$ , we must recall that, in the series expansion of the magnetic field in Eq. (7), the second linear term in the displacement was kept

apart, and it is the only term needed to obtain the magnon-phonon coupling. Thus, the remaining Hamiltonian is

$$\mathcal{H}_{mp} = -\mu_B g \sum_{ij} B_j^{\alpha\beta} S_{ij}^{\alpha} u_{ij}^{\beta}, \quad (29)$$

where the derivative is evaluated in the equilibrium position  $\mathbf{R}_j$  as established in Eq. (8).

To obtain the quantized form of the magnon-phonon Hamiltonian explicitly in  $\mathbf{k}$  space, we must start by using the Fourier transformation of  $u_i$  given in Eq. (19a). Following this, we make use of the transformations given in Eqs. (9) and (21a) and the Bloch's theorem over the magnonic creation and annihilation operators to obtain the magnetoelastic Hamiltonian in second quantization, which reads

$$\mathcal{H}_{mp} = \sum_{k\lambda j} [\Lambda_{k\lambda} a_{-kj} (c_{k\lambda} + c_{-k\lambda}^\dagger) + \text{H.c.}], \quad (30)$$

with the interaction parameter  $\Lambda_{k\lambda}$  as

$$\Lambda_{k\lambda} = -\mu_B g \sqrt{\frac{\hbar S}{4M\omega_\lambda(\mathbf{k})}} (B_j^{(x\beta)} - iB_j^{(y\beta)}) \epsilon_{k\lambda}^\beta. \quad (31)$$

From Eqs. (30) and (31), we can effectively see how a magnon-phonon coupling emerges, and that this is proportional to the magnetic field gradient. Furthermore, the magnetoelastic parameter  $\Lambda_{k\lambda}$  depends essentially on the magnitude of the derivatives of the transverse components of the magnetic field. More importantly, the gradient direction couples differently with each phonon polarization, which, in this case, correspond to the  $x$ ,  $y$ , and  $z$  axes. This last point means that, in principle, there is complete freedom to choose which phonon and magnon bands hybridize. Comparing with the usual phenomenological magnetoelastic Hamiltonian [22,23,38] given by

$$\mathcal{H}_{mp}^K = \sum_{k\lambda} [\Gamma_{k\lambda} a_{-k} (c_{k\lambda} + c_{-k\lambda}^\dagger) + \text{H.c.}], \quad (32)$$

where

$$\Gamma_{k\lambda}^K = \sqrt{\frac{\hbar B_\perp^2}{4SM\omega_p(k\lambda)}} [ik_z \epsilon_{k\lambda}^x + k_z \epsilon_{k\lambda}^y + (ik_x + k_y) \epsilon_{k\lambda}^z], \quad (33)$$

we can see that the main difference between the coupling introduced in this paper and the phenomenological one [see Eqs. (31) and (33)] is that the latter comes from an intrinsic mechanism parametrized by the magnetoelastic parameter  $B_\perp$  and it directly reflects a nonmanipulative feature of a particular material. Ultimately, this implies that there is not possibility of manipulating the magnon-polarons features as it occurs in the case of the induced magnetoelastic coupling proposed here, which even allows a control level to the point of manipulate the strength of the coupling and choosing which phonon polarizations are coupled to the magnon.

#### D. Numerical calculations

To obtain the magnon-polaron bands and properly compare the contribution of the phenomenological as the magnetic field gradient-induced magnetoelastic coupling to the system, we perform numerical calculations by employing the Colpa's [52]

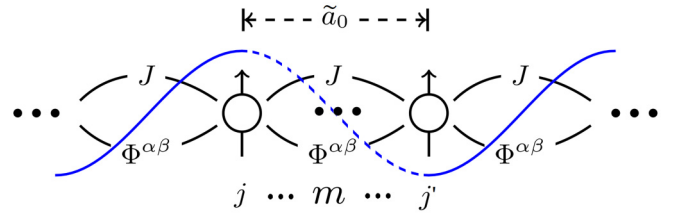


FIG. 2. Magnonic crystal characterized by a crystal lattice constant  $\tilde{a}_0$  a composed by  $m$  spins by unit cell. This is a proof of concept of the effect that the particular magnetic field gradient [see Eq. (37)] exerts on each site of the unit cell. It can be seen that the spin located at  $j$  is under an opposite force than the spin located at  $j'$ , which ultimately cancels the net force in the unit cell. This is the essence behind the feasibility of our proposal.

algorithm to para-diagonalize Hamiltonian (28). To implement the algorithm, we need to write the Hamiltonian in its quadratic form as

$$\mathcal{H} = \frac{1}{2} \sum_k [\alpha_k^\dagger \quad \alpha_{-k}] H_k [\alpha_k \quad \alpha_{-k}^\dagger]^T, \quad (34)$$

where  $\alpha_k \equiv (a_k c_{k1} c_{k2} c_{k3})$  and  $H_k$  is an  $8 \times 8$  Hermitian matrix. Colpa's algorithm [52] will return us a paraunitary matrix  $\mathcal{T}_k$  that satisfies

$$\mathcal{T}_k^\dagger H_k \mathcal{T}_k = \begin{pmatrix} E_k & 0 \\ 0 & E_{-k} \end{pmatrix}, \quad (35)$$

where  $E_k$  is a  $4 \times 4$  diagonal matrix containing the eigenenergies. The respective eigenvectors are given by

$$\begin{pmatrix} \gamma_k \\ \gamma_{-k}^\dagger \end{pmatrix} = \mathcal{T}_k \begin{pmatrix} \alpha_k \\ \alpha_{-k}^\dagger \end{pmatrix}. \quad (36)$$

### III. MAGNON-POLARON BANDS IN MAGNONIC CRYSTALS

Here, we numerically compute the magnon-polaron bands in a magnonic crystal embedded in a ferromagnetic insulator as depicted in Fig. 2 where we show a schematic of a system interacting both elastic as magnetically through  $\Phi^{\alpha\beta}$  and  $J$ , respectively, and under the action of a space-varying magnetic field. The magnonic crystal emerges when considering  $m$  ( $m > 1$ ) spins belonging to the unit cell of the system. Specifically, we use a YIG sample whose relevant parameters are listed in Table I [22,23,38]. As previously reported, periodicity on a magnetic system gives rise to the so-called magnonic crystals [53]. A magnonic crystal can be

TABLE I. Values used in the numerical calculations.

Parameter	Value
$S$	20
$M$	$9.8 \times 10^{-24}$ kg
$a_0$	12.376 Å
$v_{\parallel}$	7209 m/s
$v_{\perp}$	3843 m/s
$J$	0.24 meV

manufactured by means of periodic modulation on the magnetic anisotropy or magnetic fields [54], periodic inclusion of nonmagnetic materials [55], periodic arrays of dots [56,57], or antidots [58]. Geometrical modulations on the surface of a ferromagnetic film also gives rise to a magnonic crystal structure [59]. The main feature of the magnonic crystals is the generation of band gaps where spin waves can not propagate, allowing their manipulation for potential devices in spintronics or magnonics. Thus, a magnonic crystal can be summarized as a metamaterial that enables the suppression and/or propagation of spin waves according to its band structure. Phonons in a crystal also have a band structure, so one would expect that the hybridization between them to be magnified in terms of increasing number of anticrossing points due to the bands folding. In fact, magnon-polarons mediated by the phenomenological magnetoelastic coupling have been recently studied in similar structures [60,61].

Here, we use the arguments presented in Sec. II about the stability of the system (see also the discussion in Appendix A), which can be summarized as the absence of magnetic field gradient-induced magnon-polaron excitations when the applied magnetic field has the same periodicity of the lattice to explore the magnon-polaron excitations in magnonic crystals. Recall that the main idea behind using magnonic crystals to explore the generation of magnon-polarons mediated by a magnetic field gradients is the fact that we can modulate the magnetic field such that the force exerted by the magnetic field gradient on each unit cell belonging to the magnonic crystal is zero. In this way, we will use a periodic magnetic field, whose periodicity encodes the number of sites belongs to each unit cell. We start with a periodicity that is likely not easy to achieve experimentally but that allows us to show how our proposal should work. Next, we will go into a more realistic case and will extract some measurable effects. Let us highlight that the first case we will study is unrealistic with the current experimental techniques, but it has the advantage that allows us to show the virtues of our proposal explicitly. Importantly, the whole discussion related to the first case holds for the realistic one, which shows, in some way, how robust is our proposal.

Thus, in order to adjust the magnetic field to avoid the acceleration on the system, we will use the follow shape of it,

$$\mathbf{B}(x, z) = \left[ \frac{B^{yx}}{q_m} \sin(q_m x) + B^{yz} z \cos(q_m x) \right] \hat{y} + B^z \hat{z}, \quad (37)$$

where  $q_m = 2\pi/(ma_0)$  and  $m$  is the number of sites of the basis (see also the related case for  $m = 1$  depicted in Fig. 5). Note that  $B^{y\beta}$  ( $\beta = x, z$ ) corresponds to the derivative of the  $y$  component of the magnetic field respect to the variable  $\beta$ , according to our notation prescribed in Eq. (8). For this particular choice of the magnetic field, we can ensure that a magnetic field gradient will not produce a net force on the unit cell as long as  $m$  is an even number. Figure 2 shows with a solid blue line, the  $x$  component (modulus) of the magnetic field gradient as derived from Eq. (37) as a function of the distance along the  $x$  direction. According to our proposal, from Fig. 2, it can be seen that the exerted force driven by the magnetic field gradient on the spin located at  $j = 0$  points in the opposite direction than the exerted one on

the spin located at  $j' = 1$ , canceling, thus, the net force on the unit cell. Recall that the specific shape of the magnetic field gradient is not relevant as long as it is periodic and satisfy its nulled divergence. The choice we made in Eq. (37) is related to simplicity in our calculations and must be understood as a proof of concept. The experimental realization of such a magnetic field is beyond the scope of the present paper, however, some insights in such a direction can be found in Ref. [62].

We start by computing the magnon-polaron bands for waves propagating along the  $\hat{x}$  direction in the absence of the phenomenological magnetoelastic coupling in a magnonic crystal embedded in a YIG sample with  $m = 2$  for different values of the magnetic field gradient  $B^{y\beta}$  presented in Eq. (37), and a constant magnetic field of  $B^z = 1$  T applied into the  $\hat{z}$  direction. Note that  $m = 2$  means a crystal lattice constant  $\tilde{a}_0 \approx 24$  Å (there are two spins per unit cell), which is the atomic scale. Currently, it is not possible to obtain modulations on a magnetic field at such a scale, but, as we argued before, it is a good starting point to show the versatility of our proposal. In Figs. 3(a)–3(c), we show the magnon-polaron bands with the mentioned assumptions. The color bar is a representation of the amplitude of the probability of which character has the wave function and its corresponding eigenenergy. In this way, the green color represents essentially a magnon state, whereas the blue color represents a phonon state. The intermediate colors show how mixed are magnons and phonons, reaching the maximum coupling at the red color when  $\mathbf{k} = \mathbf{k}_i^*$ , being  $\mathbf{k}_i^*$  the  $i$ th anticrossing point. Note that the whole spectrum corresponds to magnon-polaron excitations, but, far from the anticrossing point, there excitations behave like noninteracting magnons and phonons.

Figure 3(a) shows the magnon and phonon dispersions with  $B^{yx} = 5$  T/m and  $B^{yz} = 0$ . The appearance of distinct band gaps at the crossing points is evident, which manifests the coupling between the longitudinal phonon mode with magnons propagating along the  $\hat{x}$  direction. Note that none of the transverse phonon modes couple with magnons as pointed out in Eq. (31). Also, it can be seen that due to the band folding effect, acoustic magnons might simultaneously couple with acoustic and optical phonons. Analogously, Fig. 3(b) shows the magnon-polaron bands for a magnetic field gradient applied into the  $\hat{z}$  direction with  $B^{yz} = 5$  T/m and  $B^{yx} = 0$ . Similar to the previous case, here, magnons only couple with a transverse phonon mode and again, simultaneously, couple with acoustic and optical phonons. Note that the energy band-gaps  $\Delta_i$  between the magnon-polaron modes at  $\mathbf{k}_i^*$  are different for the cases with the gradient applied into the  $\hat{x}$  and  $\hat{z}$  directions as will be shown in detail below.

Furthermore, and in order to depict the ability to control which magnon and phonon bands hybridize, Fig. 3(c) shows the system under the action of a magnetic field gradient applied into the transverse and longitudinal directions with  $B^{yz} = B^{yx} = 5$  T/m. In this case, there is a coupling of both distinct phonon modes with magnons propagating along the  $\hat{x}$  direction since the magnetic field is applied into two distinct spatial directions. If we would have considered a magnetic field gradient applied into the three spatial directions, then, the degenerated transverse phonon mode of YIG should be also coupled and, consequently, obtaining two degenerated

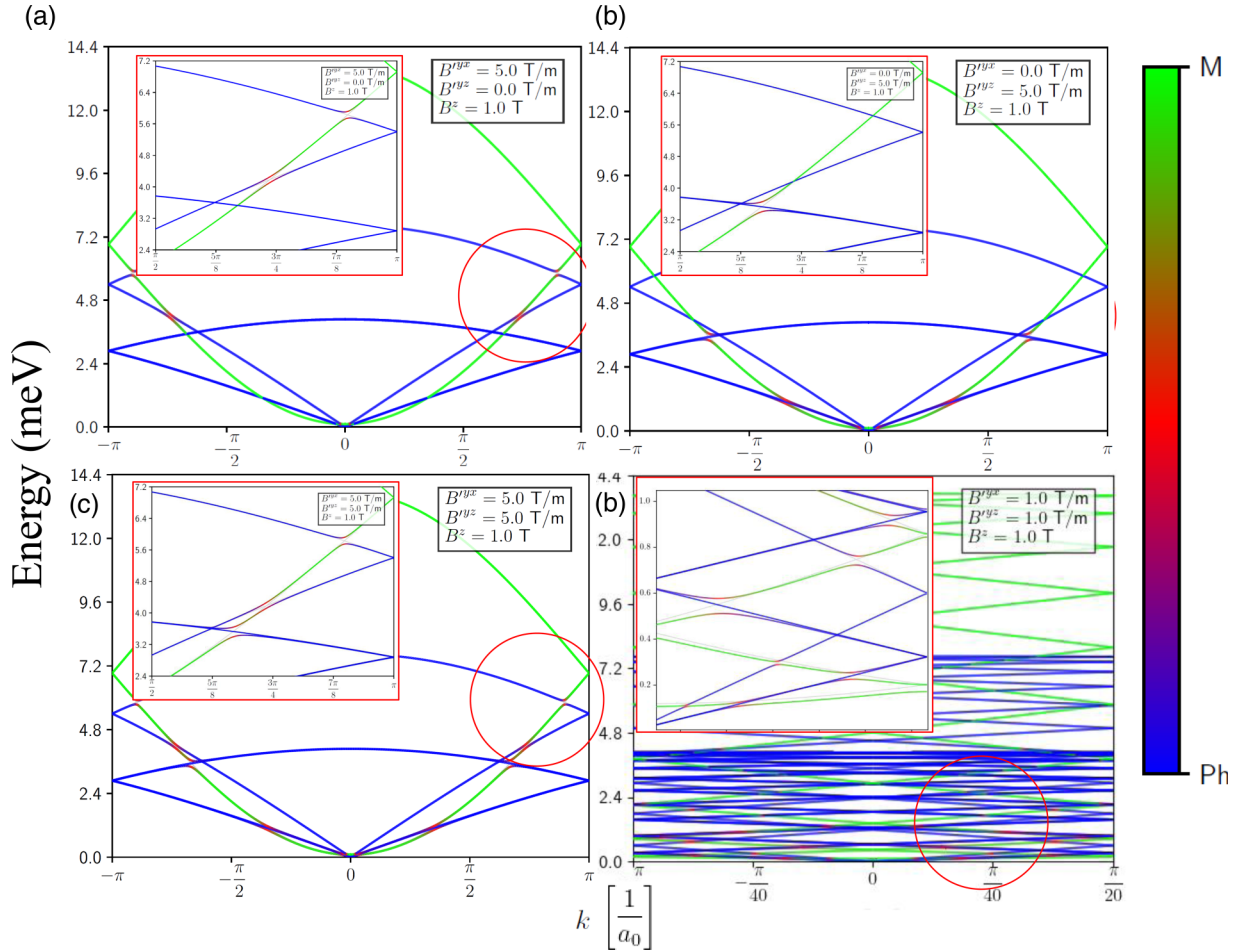


FIG. 3. Magnon-polaron bands for a YIG magnonic crystal with wave-vector  $\mathbf{k} \parallel \hat{x}$  and a magnetic field  $\mathbf{B}(x, z) = [0, B^y(x, z), 1]$  T as mentioned in the main text. In (a)–(c), the number of the sites in each unit cell is set  $m = 2$ , whereas, in (d), we set  $m = 20$ . The color bar shows the amplitude of the probability of the magnon-polaron wave function such that the green line corresponds to a quasifull magnon band, whereas the blue line corresponds to a quasifull phonon one. The maximum mixture between magnons and phonons is represented in red color. (a) Magnon-polaron bands for  $B^{yx} = 5$  T/m and  $B^{yz} = 0$ , (b) for  $B^{yx} = 0$  and  $B^{yz} = 5$  T/m, (c) for  $B^{yx} = B^{yz} = 5$  T/m; and (d)  $B^{yx} = B^{yz} = 1$  T/m. The wave-vector  $\mathbf{k} = k\hat{x}$  is written in units of  $1/a_0$ . The insets in the red boxes are a zoom in of the anticrossing points marked with a red circle.

magnon-polaron bands. In the same way, for a given material with three distinct phonon modes, a magnetic field gradient with the three spatial components gives rise to three different magnon-polaron bands. Then, we have shown that it is possible to choose which magnon-polaron mode to excite by only fixing the direction of the magnetic field gradient. Remarkably, under the same conditions as above, but considering only the phenomenological magnetoelastic coupling, the ability to choose which magnon and phonon bands interact does not exist.

Next, we go into a more realistic system by computing the magnon-polaron bands for a YIG magnonic crystal with  $m = 20$  sites per unit cell as shown in Fig. 3(d). In this case, the periodicity of the magnetic field translates into a crystal lattice constant  $\tilde{a}_0 \approx 25$  nm, which it does currently feasibly. Since  $m = 20$  means 20 magnon bands and  $2 \times 20$  phonon ones, the presented magnon-polaron bands in Fig. 3(d) shows a significant convergence between them, which makes it very difficult to distinguish them. However, it is possible to observe

the hybridization between them as depicted in red color. In this case, the calculation has been performed for a gradient of 1 T/m applied into the  $x$  and  $z$  directions, which induces a simultaneous hybridization between longitudinal and transverse phonons with magnons.

To compare the contribution of this induced magnetoelastic coupling with the usual phenomenological one, we compute the band-gap  $\Delta_i = E_k^{\text{MP}_1} - E_k^{\text{MP}_2}|_{k=k_i^*}$  that separately generates each *kind* of coupling between the magnon-polaron bands at the  $i$ th anticrossing point  $k_i^*$  and using the same parameters as above, i.e., a YIG magnonic crystal with  $m = 20$ . Thus, in Fig. 4, we have plotted, on a log-log scale, the energy gap  $\Delta$  for different values of the magnetic field gradient  $B^{y\beta}$  ( $\beta = x, z$ ), where we have considered only the two lowest pairs of magnon-polaron bands. As stated above, the gap is measured at all the possible wave-vectors  $\mathbf{k} = \mathbf{k}^*$  where the magnon and phonon bands would cross in the absence of magnetoelastic coupling and have been depicted by solid and dashed lines according the coupled phonon mode. Specifically, the solid lines



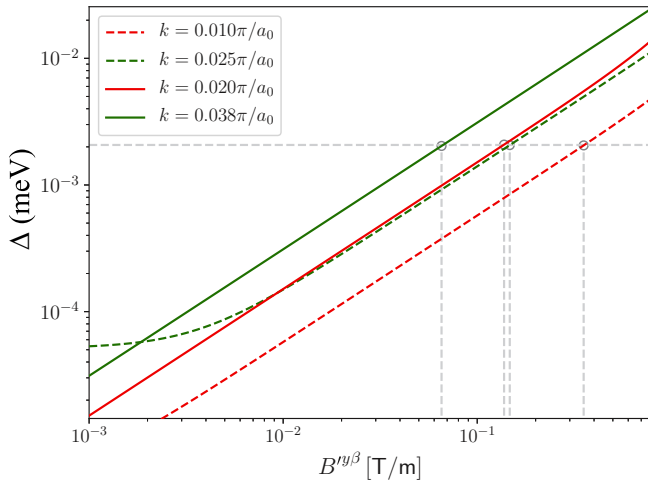


FIG. 4. Energy gap for different values of the magnetic field gradients  $B^{y\beta}$  presented in Eq. (37) in the main text for a YIG magnonic crystal with a basis  $m = 20$ . The presented values are obtained by computing the two lowest pairs of magnon-polaron bands [see Fig. 3(d)]. The red color is used to represent the band gap between the lowest pair of magnon-polaron bands (acoustic magnons coupled with acoustic phonons), and the green color is used to represent the energy band gap between the next pair of magnon-polaron bands (optical magnons coupled with acoustic phonons). In the solid and dashed lines, it is shown the gap between magnons and transverse and longitudinal phonon modes, respectively. The gray horizontal line represents the energy gap  $\Delta_K$  obtained in Ref. [23].

represent coupling between magnons and transverse phonon modes, whereas the dashed lines correspond to coupling between magnons and longitudinal phonon modes. The red and green colors are used to show in which anticrossing point  $k_i^*$  is measured the energy band gap. More precisely, the coupling between acoustic magnons and phonons is depicted with the red lines, whereas the coupling between acoustic magnons and optical phonons are represented by green lines (see Fig. 4 for comparison). In this plot, the log-log scale has been used to show the energy gap for a wide range of magnetic field gradients, however, we have also performed a linear plot depicted in Appendix B in Fig. 6. It is of particular interest to find the value of  $B^{y\beta}$  for which each gap reproduces the gap seen in Ref. [23], which is approximately  $\Delta_K \approx 2.1 \mu\text{eV}$ , an aspect that has been marked by the gray dotted lines. The importance of reproducing such a gap by means of the current proposal relies on the fact that most of the experimental measurements have been accomplished in YIG samples by only considering the phenomenological contribution.

From Fig. 4, we can also see with the solid red line that acoustic magnons couple with transverse acoustic phonons at  $k_{\perp 1}^* \approx 5.07 \times 10^7 \text{ m}^{-1}$ , whereas optical magnons couple transverse acoustic phonons at  $k_{\perp 2}^* \approx 9.64 \times 10^7 \text{ m}^{-1}$  as depicted with a solid green line. Similarly, Fig. 4 also shows that, at  $k_{\parallel 1}^* \approx 2.53 \times 10^7 \text{ m}^{-1}$ , acoustic magnons and a longitudinal acoustic phonon mode are coupled, whereas, at  $k_{\parallel 2}^* \approx 6.34 \times 10^7 \text{ m}^{-1}$ , optical magnons couple with the transverse acoustic phonon band. Note that the gap opened at  $k_{\parallel 2}^*$  has a nontrivial behavior with the magnetic field gradient. In fact,

for gradient values smaller than  $\sim 10^{-2} \text{ T/m}$ , the gap does not have significant dependence on the magnetic field gradient but, then, grows almost linearly for higher values of it. We attribute this behavior to the high number of bands converging in a small portion of the phase space for small values of the magnetic field gradient, making the population of magnon-polarons profoundly affected by the contiguous hybridizations. Importantly, the gap reproduced in Ref. [23]  $\Delta_K$  can be reproduced with magnetic field gradients of about  $\sim 0.1 \text{ T/m}$ , that, in fact, can be reasonably achieved with the current experimental techniques [63–67]. Indeed, by using a magnetic microtrap, Ref. [62] reported gradients of up to  $8000 \text{ T/m}$ , which, due to the linear behavior of  $\Delta$  with  $B^{\alpha\beta}$  (see related discussion in Appendix B), it would translate into very large  $\Delta$  values, so we predict enhancements of transport properties related to the presence of magnon-polarons when a magnetic field gradient larger than  $0.1 \text{ T/m}$  is applied. Interestingly, Fig. 4 (see also Fig. 6) also shows that we could reach gaps of order of about  $0.1 \text{ meV}$  with gradients of about  $\sim 10 \text{ T/m}$ . This gap is on the same order as reported on previous works on topological magnonics [68].

#### IV. CONCLUSIONS

In this paper, we have proposed a versatile way to induce a magnetoelastic coupling in any (anti)ferromagnetic material. Despite the fact that our formalism was developed in a specific spin chain, it can be extended to more sophisticated systems where we expect similar behaviors due to the generalized treatment we gave for the total Hamiltonian. The main contribution of the present paper is the proposal of an enhancement of the magnetoelastic coupling by a magnetic field gradient. The physics behind it can be understood in terms of the force exerted by the magnetic field gradient on each magnetic dipole which deviates them from its equilibrium position exciting, thus, simultaneously, both phonon and magnon modes. Importantly, for a realistic setup (represented by  $m = 20$  in our calculations), the order of magnitude of the magnetic field gradient needed to achieve measurable effects starts from  $\sim 10^{-1} \text{ T/m}$  in YIG, which is well accomplished in standard experiments. Since a magnetic field gradient means an external force on each magnetic dipole, an infinite system with the same periodicity of the magnetic field is then accelerated and a non-Hermitian Hamiltonian is expected when considering the  $\hat{z}$  axis as the ground state, so no magnon-polarons can be excited. This can be overcome by properly adjusting the magnetic field periodicity such that the net force on each unit cell of the system is zero. Thus, by employing our proposal in a magnonic crystal where the nature of it allows having such features, we can avoid the imaginary parts of the energy spectrum and real energies are obtained in the whole Brillouin zone. Furthermore, as a highlighted results, the band gaps in the magnonic crystal can be controlled by varying the strength and direction of the magnetic field gradient. Note that since the formalism demands a stable ground state in the system, which must be accomplished canceling the net force emerged from the gradient on the unit cell of the system, our proposal should be very well achieved in an antiferromagnetic system where the nature of the unit cell would allow major liberty on the choice of the magnetic field shape. In such a case, since

forces emerged from the magnetic field gradient leads to local deformations, we should first compute the new equilibrium positions and, then, perform the whole analysis developed in this paper. Finally, our proposal could open new possibilities to control the magnon-phonon interaction with the idea of manufacturing efficient spintronic and/or magnonics devices. We claim, then, that this induced magnetoelastic coupling is fully controllable by a magnetic field gradient. Since most of magnon-polaron transport properties depend on the strength of this interaction, we predict, thus, an enhancement of them by controlling the strength and direction of the magnetic field gradient.

### ACKNOWLEDGMENTS

N.V.-S. thanks K. Shen for fruitful discussions and Fondecyt Postdoctorado Grant No. 3190264. A.S.N. thanks Fondecyt Regular Grant No. 1190324. N.V.-S., A.S.N., and E.A. thank Financiamiento Basal para Centros Científicos y Tecnológicos de Excelencia AFB180001. This project has received funding from the European Research Council (ERC) under the European Union's Horizon 2020 Research and Innovation Programme (Grant Agreement No. 725509).

### APPENDIX A: EQUILIBRIUM CONDITION IN AN ARBITRARY LATTICE

To analyze the equilibria in an arbitrary lattice, let us first start by analyzing the equilibrium in a system composed of a single spin attached to a spring and coupled to a inhomogeneous magnetic, whose Hamiltonian is described by

$$\mathcal{H} = \frac{\mathbf{p}^2}{2M} + \frac{M\omega_0^2}{2}\mathbf{u}^2 - \mu_B g \mathbf{B} \cdot \mathbf{S}, \quad (\text{A1})$$

where we have defined the small deviation  $\mathbf{u} = (x - X_0)\hat{\mathbf{x}}$ , being  $X_0$  the equilibrium position. Classically, the spin's time evolution is governed by Newton's second law and the Landau-Lifschitz-Gilbert equation. To make the study of the system's equilibria more comfortable, the spin variable can be written in spherical coordinates angles  $\theta, \phi$ , and it can be considered the particular case where  $\mathbf{B} = [0, B^y(x), B^z]$ , meaning that the classical energy  $E(x, \theta, \phi)$  is given by

$$E(x, \theta, \phi) = \frac{\mathbf{p}^2}{2M} + \frac{M\omega_0^2}{2}\mathbf{u}^2 - \mu_B g S B^y \sin(\theta) \sin(\phi) - \mu_B g S B^z \cos(\theta). \quad (\text{A2})$$

From Eq. (A2), the equilibria of the system follow directly from minimizing the energy. For this, it must be imposed that  $\partial_x E = 0$ ,  $\partial_\theta E = 0$ , and  $\partial_\phi E = 0$ ,

$$M\omega_0^2 u - \mu_B g S \frac{\partial B^y}{\partial x} \sin(\theta) \sin(\phi) = 0, \quad (\text{A3a})$$

$$B^y \cos(\theta) \sin(\phi) - B^z \sin(\theta) = 0, \quad (\text{A3b})$$

$$B^y \sin(\theta) \cos(\phi) = 0. \quad (\text{A3c})$$

From Eq. (A3), it is direct to see that  $(u, \theta, \phi) = (0, 0, 0)$  is a solution. Studying the Hessian at the equilibrium point, it is clear that this is positive definite whenever the following inequality complies:

$$\left( \frac{\partial B^y}{\partial x} \Big|_{u=0} \right)^2 < \frac{M\omega_0^2}{g\mu_B S} B^z. \quad (\text{A4})$$

Thus, the point  $(u, \theta, \phi) = (0, 0, 0)$  is a stable equilibrium whenever the condition established by inequality (A4) is fulfilled. The importance of analyzing the equilibrium of Hamiltonian (A1) comes from the fact that the equilibrium needs to be stable for it to have spin waves. This single spin-toy model allows us to see that there exists a magnetic field gradient from which the equilibrium is no longer stable and no spin waves are admitted under those conditions.

Now, we go beyond this single spin model and expand our analysis of equilibrium to an extended one-dimensional lattice with the spacing  $a_0$  parameter. The simplest system with both magnetic and elastic interactions is given by

$$\mathcal{H} = \sum_i \left[ \frac{\mathbf{p}_i^2}{2M} + \frac{M\omega_0^2}{2}(\mathbf{u}_{i+1} - \mathbf{u}_i)^2 - JS_i \cdot \mathbf{S}_{i+1} - \mu_B g \mathbf{B} \cdot \mathbf{S}_i \right], \quad (\text{A5})$$

where the unidimensional elastic interaction and Heisenberg exchange were considered. To further simplify the model, the magnetic field  $\mathbf{B}(x)$  will be assumed to be periodic with a periodicity equal to that of the lattice. Next, we expand the arbitrary magnetic field  $\mathbf{B}(x)$  around the equilibrium positions  $\mathbf{X}_i$  up to first order in the displacement  $\mathbf{u}$ , which leads to

$$\mathcal{H} = \sum_i \left[ \frac{\mathbf{p}_i^2}{2M} + \frac{M\omega_0^2}{2}(\mathbf{u}_{i+1} - \mathbf{u}_i)^2 - JS_i \cdot \mathbf{S}_{i+1} - \mu_B g \mathbf{B} \cdot \mathbf{S}_i - \mu_B g \frac{\partial \mathbf{B}}{\partial x^\mu} \cdot \mathbf{S}_i u^\mu \right], \quad (\text{A6})$$

where the positions  $\mathbf{X}_i = (ia_0, 0, 0)$  and the spin ground-state  $\mathbf{S}_i = (0, 0, S)$  were chosen as possible equilibria of the system.

To study the actual equilibria of Hamiltonian (A5), the spin variable will be written in terms of its spherical angles  $\theta_i$  and  $\phi_i$  and, as in the single spin case, it will be assumed that the magnetic field is given by  $\mathbf{B} = [0, B^y(x), B^z]$ . With these considerations, the Hamiltonian can be written explicitly as

$$\mathcal{H} = \sum_i \left\{ \frac{\mathbf{p}_i^2}{2M} + \frac{M\omega_0^2}{2}(\mathbf{u}_{i+1} - \mathbf{u}_i)^2 - JS^2 [\sin(\theta_i) \sin(\theta_{i+1}) \cos(\phi_i) \cos(\phi_{i+1}) + \sin(\theta_i) \sin(\theta_{i+1}) \sin(\phi_i) \sin(\phi_{i+1}) + \cos(\theta_i) \cos(\theta_{i+1})] - \mu_B g [SB^y(x) \sin(\theta_i) \sin(\phi_i) + SB^z \cos(\theta_i)] \right\}. \quad (\text{A7})$$

Using the single spin case as inspiration, the point  $(u_i, \theta_i, \phi_i) = (0, 0, \pi/2)$  is considered as possible equilibrium. We expand the Hamiltonian (A7) to second order around the mentioned point,

$$\mathcal{H} = \sum_i \left[ \frac{\mathbf{p}_i^2}{2M} + \frac{M\omega_0^2}{2}(\mathbf{u}_{i+1} - \mathbf{u}_i)^2 - JS^2 (\theta_i \theta_{i+1} - \theta_i^2 - \theta_{i+1}^2) - \mu_B g S \left( \frac{\partial B^y}{\partial x} u_i \theta_i - B^z \theta_i^2 \right) \right]. \quad (\text{A8})$$

To find the stability of the system, Fourier's theorem on  $u_i$  and  $\theta_i$  will be used. This will lead to a Hamiltonian described by  $u_k$ ,  $u_{-k}$ ,  $\theta_k$ , and  $\theta_{-k}$ , which is given by

$$\mathcal{H} = \sum_k \left[ \frac{p_k^2}{2M} + M\omega_0^2[1 - \cos(ka)]u_k u_{-k} - 2JS^2[1 - \cos(ka)]\theta_k \theta_{-k} + \mu_B g S B^z \theta_k \theta_{-k} - \mu_B g S \frac{\partial B^y}{\partial x} u_k \theta_{-k} \right]. \quad (\text{A9})$$

From the Hamiltonian in  $k$  space, it can be noted that the Hessian is a block diagonal matrix where each block is  $4 \times 4$ , formed by the variables  $u_k$ ,  $\theta_k$ ,  $u_{-k}$ , and  $\theta_{-k}$ . With this, it can be proved that every eigenvalue is positive if and only if

$$\left( \frac{\partial B^y}{\partial x} S g \mu_B \right)^2 < 4MS\omega_0^2 \{-2JS[1 - \cos(ak)] + \mu_B g B^z\} \sin^2 \left( \frac{ak}{2} \right), \quad (\text{A10})$$

which is Eq. (4) of the main text. As an extra note, it is essential to recognize that, intuitively, the proposed equilibrium could never be stable because every site feels the same force, thus, always pushing it away from the equilibrium obtained with a constant magnetic field. As explained in Sec. IID of the main text, the way we choose to diagonalize the Hamiltonian of the system is following the Colpa's algorithm, which demands to write the total Hamiltonian into its quadratic form. However, as shown in Eq. (A10), there will be some range of  $k$  values where the diagonalization procedure breaks down essentially because of the system is no longer stable at the chosen equilibrium points. In order to show explicitly such a claim, in Fig. 5, we compute the magnon-polaron bands for a magnetic field given by

$$\mathbf{B}(x) = B_y \sin \left( \frac{2\pi}{a_0} x \right) \hat{y}, \quad (\text{A11})$$

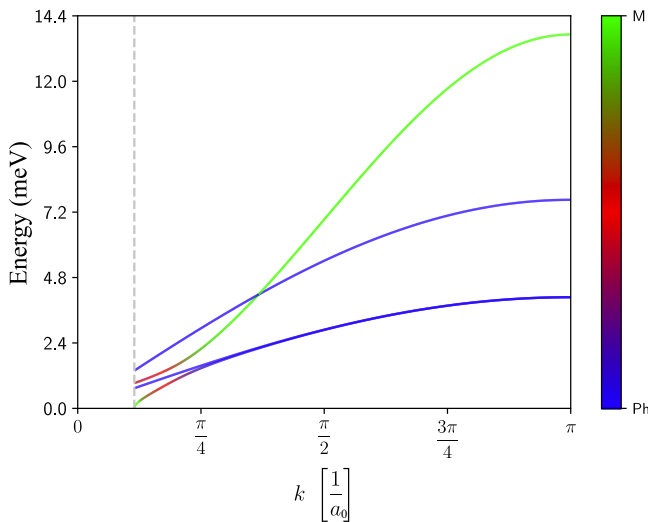


FIG. 5. Magnon-polaron bands for a YIG sample as function of  $1/a_0$  for  $B_y = 1$  nT. The green color is used to denote the probability amplitude of the eigenstate to be a magnon and blue is used to denote any phonon mode. The gray-dotted vertical line denotes the point when the Hamiltonian is no longer positive definite and no physical eigenenergies are observed below it.

where it must be noted that  $\mathbf{B}(x)$  has the same periodicity of the lattice, in the same way as assumed to arrive in Eq. (A10). Also, the magnetic field gradient has been applied into the  $x$  direction, it has been used  $B_y = 1$  nT, and the magnetic parameters were extracted from Table I for a YIG sample. Importantly, the gray-dotted vertical line marks the point where inequality (A10) stops being true. Thus, it has been proven that when applying a magnetic field gradient on a magnetic field with the same periodicity of the lattice, the system feels a net force which ultimately accelerates it and is no longer stable. This has the consequence of magnon-polaron excitations should not be observed for this case.

#### APPENDIX B: ENERGY GAP $\Delta$ AS A FUNCTION OF THE MAGNETIC FIELD GRADIENT

Here, we show the dependence of the energy gap  $\Delta$  as a function of the magnetic field gradient. As depicted in Fig. 4 of the main text, the log-log scale was used to show a wide range of the magnetic field gradient. However, here, we use a linear scale to show that the energy gap  $\Delta$  effectively varies linearly with  $B^{y\beta}$  from values of  $B^{y\beta}$  larger than  $\sim 0.1$  T/m as shown in Fig. 6.

The most important aspect of Fig. 6 is that a linear equation can directly describe it:  $\Delta = bB^{y\mu}$  ( $\mu = \alpha, \beta$ ), and the log-log scale is not necessary to show the linear behavior of the energy gap but was, nonetheless, used to clearly show in the same plot the value upon which the gap in Ref. [23] is obtained.

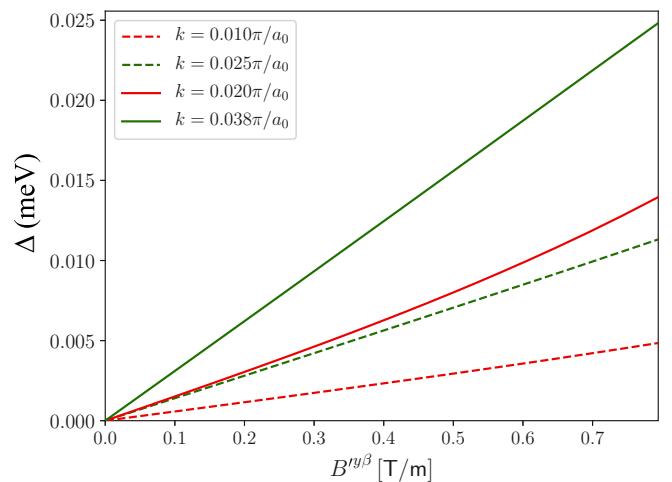


FIG. 6. Energy band-gap  $\Delta$  as a function of the magnetic field gradient  $B^{y\alpha}$  as depicted in Fig. 4. In this case, the linear scale has been used.

- [1] I. Žutić, J. Fabian, and S. D. Sarma, *Rev. Mod. Phys.* **76**, 323 (2004).
- [2] S. Bader and S. Parkin, *Annu. Rev. Condens. Matter Phys.* **1**, 71 (2010).
- [3] A. V. Chumak, V. I. Vasyuchka, A. A. Serga, and B. Hillebrands, *Nat. Phys.* **11**, 453 (2015).
- [4] V. Kruglyak, S. Demokritov, and D. Grundler, *J. Phys. D: Appl. Phys.* **43**, 264001 (2010).
- [5] A. Serga, A. Chumak, and B. Hillebrands, *J. Phys. D: Appl. Phys.* **43**, 264002 (2010).
- [6] G. E. Bauer, E. Saitoh, and B. J. Van Wees, *Nature Mater.* **11**, 391 (2012).
- [7] M. Matsuo, E. Saitoh, and S. Maekawa, *J. Phys. Soc. Jpn.* **86**, 011011 (2017).
- [8] A. Akhiezer, V. Bar'iskhtar, and S. Peletminskii, *Sov. Phys. JETP* **35**(8), 1 (1959).
- [9] R. Q. Scott and D. Mills, *Phys. Rev. B* **15**, 3545 (1977).
- [10] E. Abrahams and C. Kittel, *Phys. Rev.* **88**, 1200 (1952).
- [11] C. Kittel and E. Abrahams, *Rev. Mod. Phys.* **25**, 233 (1953).
- [12] C. Kittel, *Phys. Rev.* **110**, 836 (1958).
- [13] D. A. Bozhko, V. I. Vasyuchka, A. V. Chumak, and A. A. Serga, *Low Temp. Phys.* **46**, 383 (2020).
- [14] S. Park, N. Nagaosa, and B.-J. Yang, *Nano Lett.* **20**(4), 2741 (2020).
- [15] X. Zhang, Y. Zhang, S. Okamoto, and D. Xiao, *Phys. Rev. Lett.* **123**, 167202 (2019).
- [16] C. Berk, M. Jaris, W. Yang, S. Dhuey, S. Cabrini, and H. Schmidt, *Nat. Commun.* **10**, 1 (2019).
- [17] D. D. Stancil and A. Prabhakar, *Spin Waves* (Springer US, New York, 2009), Vol. 5.
- [18] R. Orbach, *Phys. Rev.* **115**, 1181 (1959).
- [19] G. P. Srivastava, *The Physics of Phonons* (Routledge, Abingdon-Thames, U.K., 2019).
- [20] A. G. Gurevich and G. A. Melkov, *Magnetization Oscillations and Waves* (CRC, Boca Raton, FL, 1996).
- [21] S. C. Guerreiro and S. M. Rezende, *Phys. Rev. B* **92**, 214437 (2015).
- [22] A. Rückriegel, P. Kopietz, D. A. Bozhko, A. A. Serga, and B. Hillebrands, *Phys. Rev. B* **89**, 184413 (2014).
- [23] B. Flebus, K. Shen, T. Kikkawa, K. Uchida, Z. Qiu, E. Saitoh, R. A. Duine, and G. E. W. Bauer, *Phys. Rev. B* **95**, 144420 (2017).
- [24] A. Kamra, H. Keshtgar, P. Yan, and G. E. W. Bauer, *Phys. Rev. B* **91**, 104409 (2015).
- [25] K. Shen and G. E. W. Bauer, *Phys. Rev. Lett.* **115**, 197201 (2015).
- [26] T. Kikkawa, K. Shen, B. Flebus, R. A. Duine, K. Uchida, Z. Qiu, G. E. W. Bauer, and E. Saitoh, *Phys. Rev. Lett.* **117**, 207203 (2016).
- [27] R. Yahiro, T. Kikkawa, R. Ramos, K. Oyanagi, T. Hioki, S. Daimon, and E. Saitoh, *Phys. Rev. B* **101**, 024407 (2020).
- [28] L. J. Cornelissen, K. Oyanagi, T. Kikkawa, Z. Qiu, T. Kuschel, G. E. W. Bauer, B. J. van Wees, and E. Saitoh, *Phys. Rev. B* **96**, 104441 (2017).
- [29] B. Zare Rameshti and R. A. Duine, *Phys. Rev. B* **99**, 060402(R) (2019).
- [30] G. Go, S. K. Kim, and K.-J. Lee, *Phys. Rev. Lett.* **123**, 237207 (2019).
- [31] S. Zhang, G. Go, K.-J. Lee, and S. K. Kim, *Phys. Rev. Lett.* **124**, 147204 (2020).
- [32] E. Thingstad, A. Kamra, A. Brataas, and A. Sudbø, *Phys. Rev. Lett.* **122**, 107201 (2019).
- [33] P. Shen and S. K. Kim, *Phys. Rev. B* **101**, 125111 (2020).
- [34] H. T. Simensen, R. E. Troncoso, A. Kamra, and A. Brataas, *Phys. Rev. B* **99**, 064421 (2019).
- [35] A. S. Sukhanov, M. S. Pavlovskii, P. Bourges, H. C. Walker, K. Manna, C. Felser, and D. S. Inosov, *Phys. Rev. B* **99**, 214445 (2019).
- [36] H. Hayashi and K. Ando, *Phys. Rev. Lett.* **121**, 237202 (2018).
- [37] T. Nomura, X.-X. Zhang, S. Zherlitsyn, J. Wosnitza, Y. Tokura, N. Nagaosa, and S. Seki, *Phys. Rev. Lett.* **122**, 145901 (2019).
- [38] S. Streib, N. Vidal-Silva, K. Shen, and G. E. W. Bauer, *Phys. Rev. B* **99**, 184442 (2019).
- [39] S. Streib, H. Keshtgar, and G. E. W. Bauer, *Phys. Rev. Lett.* **121**, 027202 (2018).
- [40] S. F. Maehrlein, I. Radu, P. Maldonado, A. Paarmann, M. Gensch, A. M. Kalashnikova, R. V. Pisarev, M. Wolf, P. M. Oppeneer, J. Barker *et al.*, *Sci. Adv.* **4**, eaar5164 (2018).
- [41] J. Holanda, D. Maior, A. Azevedo, and S. Rezende, *Nat. Phys.* **14**, 500 (2018).
- [42] E. Schlömann and R. Joseph, *J. Appl. Phys.* **35**, 2382 (1964).
- [43] W. Strauss, *Physical Acoustics* (Elsevier, Amsterdam, 1968).
- [44] S. Rezende and F. Morgenthaler, *J. Appl. Phys.* **40**, 537 (1969).
- [45] K. Shen, *Phys. Rev. B* **99**, 024417 (2019).
- [46] R. Ramos, T. Hioki, Y. Hashimoto, T. Kikkawa, P. Frey, A. Kreil, V. Vasyuchka, A. Serga, B. Hillebrands, and E. Saitoh, *Nat. Commun.* **10**, 1 (2019).
- [47] C. Calero, E. M. Chudnovsky, and D. A. Garanin, *Phys. Rev. Lett.* **95**, 166603 (2005).
- [48] T. Holstein and H. Primakoff, *Phys. Rev.* **58**, 1098 (1940).
- [49] S. Toth and B. Lake, *J. Phys.: Condens. Matter* **27**, 166002 (2015).
- [50] S. Blundell, *Magnetism in Condensed Matter*, Oxford Master Series in Physics (Oxford University Press, Oxford, 2003).
- [51] M. P. Marder, *Condensed Matter Physics* (Wiley, Hoboken, New Jersey, 2010).
- [52] J. Colpa, *Physica A* **93**, 327 (1978).
- [53] A. Chumak, A. Serga, and B. Hillebrands, *J. Phys. D: Appl. Phys.* **50**, 244001 (2017).
- [54] R. E. Troncoso, C. Ulloa, F. Pesce, and A. S. Nunez, *Phys. Rev. B* **92**, 224424 (2015).
- [55] G. Centała, M. L. Sokolovskyy, C. S. Davies, M. Mruczkiewicz, S. Mamica, J. Rychły, J. W. Klos, V. V. Kruglyak, and M. Krawczyk, *Phys. Rev. B* **100**, 224428 (2019).
- [56] G. Gubbiotti, S. Tacchi, M. Madami, G. Carlotti, S. Jain, A. Adeyeye, and M. Kostylev, *Appl. Phys. Lett.* **100**, 162407 (2012).
- [57] S. Tacchi, M. Madami, G. Gubbiotti, G. Carlotti, H. Tanigawa, T. Ono, and M. P. Kostylev, *Phys. Rev. B* **82**, 024401 (2010).
- [58] H. Ulrichs, B. Lenk, and M. Münzenberg, *Appl. Phys. Lett.* **97**, 092506 (2010).
- [59] R. A. Gallardo, T. Schneider, A. Roldán-Molina, M. Langer, J. Fassbender, K. Lenz, J. Lindner, and P. Landeros, *Phys. Rev. B* **97**, 144405 (2018).



- [60] P. Graczyk, J. Kłos, and M. Krawczyk, *Phys. Rev. B* **95**, 104425 (2017).
- [61] P. Graczyk and M. Krawczyk, *Phys. Rev. B* **96**, 024407 (2017).
- [62] J. Reichel, W. Hänsel, and T. W. Hänsch, *Phys. Rev. Lett.* **83**, 3398 (1999).
- [63] P. Kunert, D. Georgen, L. Bogunia, M. Baig, M. Baggash, M. Johanning, and C. Wunderlich, *Appl. Phys. B* **114**, 27 (2014).
- [64] M. Johanning, A. Braun, N. Timoney, V. Elman, W. Neuhauser, and C. Wunderlich, *Phys. Rev. Lett.* **102**, 073004 (2009).
- [65] J. Welzel, A. Bautista-Salvador, C. Abarbanel, V. Wineman-Fisher, C. Wunderlich, R. Folman, and F. Schmidt-Kaler, *Eur. Phys. J. D* **65**, 285 (2011).
- [66] A. Khromova, C. Piltz, B. Scharfenberger, T. F. Gloger, M. Johanning, A. F. Varón, and C. Wunderlich, *Phys. Rev. Lett.* **108**, 220502 (2012).
- [67] F. Mintert and C. Wunderlich, *Phys. Rev. Lett.* **87**, 257904 (2001).
- [68] S. A. Díaz, J. Klinovaja, and D. Loss, *Phys. Rev. Lett.* **122**, 187203 (2019).